

Intraseasonal variability of sea level and circulation in the Gulf of Thailand: the role of the Madden–Julian Oscillation

Eric C. J. Oliver

Received: 23 August 2012 / Accepted: 7 November 2012
© Springer-Verlag Berlin Heidelberg 2012

Abstract Intraseasonal variability of the tropical Indo-Pacific ocean is strongly related to the Madden–Julian Oscillation (MJO). Shallow seas in this region, such as the Gulf of Thailand, act as amplifiers of the direct ocean response to surface wind forcing by efficient setup of sea level. Intraseasonal ocean variability in the Gulf of Thailand region is examined using statistical analysis of local tide gauge observations and surface winds. The tide gauges detect variability on intraseasonal time scales that is related to the MJO through its effect on local wind. The relationship between the MJO and the surface wind is strongly seasonal, being most vigorous during the monsoon, and direction-dependent. The observations are then supplemented with simulations of sea level and circulation from a fully nonlinear barotropic numerical ocean model (Princeton Ocean Model). The numerical model reproduces well the intraseasonal sea level variability in the Gulf of Thailand and its seasonal modulations. The model is then used to map the wind-driven response of sea level and circulation in the entire Gulf of Thailand. Finally, the predictability of the setup and setdown signal is discussed by relating it to the, potentially predictable, MJO index.

Keywords Madden–Julian Oscillation · Predictability · Wind-driven circulation · Shelf circulation

1 Introduction

The ability to predict ocean variability on intraseasonal time scales has been an area of increased focus in recent decades. Intraseasonal variations are of particular interest as they provide a bridge between weather variability, which occurs on timescales less than about two weeks, and climate variability, which occurs on much longer timescales. These variations may provide unprecedented predictability for long-range weather forecasts and for operational oceanographic applications. Recently, the ability to run high-resolution circulation models, for both the ocean and the atmosphere, have led to a number of studies of intraseasonal ocean variability and its predictability.

The most well-known source of intraseasonal variations in the ocean-atmosphere system is the Madden–Julian Oscillation (MJO, Madden and Julian 1971, 1972). The MJO originates over the tropical Indian Ocean as anomalous precipitation, deep convection and zonal wind. These anomalies then propagate eastward along the equator and are strongest over the Indian Ocean and Western Pacific Ocean before dissipating over the Eastern Pacific, the Atlantic Ocean, or Africa. The MJO is the dominant mode of intraseasonal variability in the tropical atmosphere and is quasi-periodic on timescales between 30 and 90 days with peak energy at periods around 40–50 days (e.g., Wheeler and Hendon 2004; Zhang 2005).

The MJO is characterized as an atmospheric phenomenon but has been shown to have a significant influence on ocean variability as well. Connections have been found with sea surface temperature (e.g., Shinoda et al. 1998; Maloney and Kiehl 2002; Maloney et al. 2008) and sea level (e.g., Fu 2003, 2007; Oliver and Thompson 2010; Webber et al. 2010). Oliver and Thompson (2010) showed that sea level variability in several ocean regions, including

E. C. J. Oliver (✉)
Institute for Marine and Antarctic Studies,
University of Tasmania, Hobart, TAS, Australia
e-mail: eric.oliver@utas.edu.au

the equatorial Pacific, the west coast of the American continent, the Gulf of Carpentaria, and the northeastern Indian Ocean, have strong connections with MJO variability. Han et al. (2001), Han (2005), Iskandar et al. (2005), Nagura and McPhaden (2012) examined intraseasonal variability in Indian Ocean circulation and Oliver and Thompson (2010) speculated on the role of MJO-related surface wind in exciting the observed response. Webber et al. (2010) also noted the connections between the MJO and sea level and sea surface temperature in the equatorial Pacific and Indian Oceans. The Madden–Julian Oscillation has even been shown to influence ocean temperature and salinity at depth (Matthews et al. 2010), surface chlorophyll (Jin et al. 2012), and possibly ocean variability as far from the tropics as coastal Chile (Hormazabal et al. 2002).

Classical wind setup predicts that the sea level setup at the coast is proportional to onshore wind stress. It is derived from a simple force balance between onshore wind stress and the pressure gradient associated with the sea level slope (e.g., Csanady 1982). Classical wind setup is an approximation with many limitations (e.g., it neglects bottom stress and horizontal fluid transport) but allows for a simple examination of the first-order response of coastal sea level to surface wind forcing. Sea level variations in large shallow seas are particularly responsive to this effect since wind setup is proportional to the fetch length and inversely proportional to water depth. Oliver and Thompson (2011) found that intraseasonal sea level variations in the Gulf of Carpentaria were largely driven by the MJO-related surface wind stress. The MJO-wind connection was shown to vary seasonally with the influence of the MJO being strongest when it modulated the monsoon-related winds in Austral Summer. This connection was also strongest for wind directions that were favourable for sea level setup and setdown in the Gulf of Carpentaria. The MJO was shown to be responsible for predictable variations in sea level up to 6 cm in amplitude.

The Gulf of Thailand is a shallow sea which, like the Gulf of Carpentaria, lies within the tropical regions strongly influenced by the MJO. It has been noted that wind forcing is the dominant factor in generating the observed circulation in the Gulf of Thailand (e.g., Ascharyaphotha et al. 2008). In a broader study of the South China Sea, Zhuang et al. (2010) found that the Gulf of Thailand is sensitive to intraseasonal variability in surface winds. They also noted that intraseasonal sea level variability could largely be explained as barotropic adjustment to surface forcing. They suggested that, due to seasonal changes in stratification and the amplitude of intraseasonal wind forcing, the intraseasonal sea level variability is largely driven by surface forcing in winter and this connection is weaker in spring and fall and nearly nonexistent in summer. Furthermore, an MJO-related sea level signal in

the Gulf of Thailand was noted by Oliver (2011) while examining the influence of the MJO in the northeastern Indian Ocean. Therefore, we expect MJO-related surface winds to play a significant role in forcing sea level and circulation in the Gulf of Thailand on intraseasonal time scales.

Sea level variations, and the associated circulation pattern, may be related to changes in nutrient levels or biological productivity in the Gulf, due to upwelling or advection from neighbouring regions, and may modify the flushing time of pollutants from the Gulf. Intraseasonal sea level variability may also be important for coastal communities when superimposed on other changes such as storm surges or global sea level rise. Therefore, accurate predictions of sea level variations, on all time scales, may lead to more accurate predictions of the greater marine system.

In this study we examine the effect of the MJO on sea level and circulation variability in the Gulf of Thailand, henceforth referred to as the Gulf. Earlier studies raised the issue of seasonal stratification changes influencing the response of sea level in the Gulf on intraseasonal time scales. We test if the observed sea level variability can be reproduced without such seasonal changes in stratification and then extend the analysis to include depth-averaged circulation variability. We accomplish this using a regional barotropic ocean circulation model validated by comparison with coastal tide gauge observations. On intraseasonal timescales, the ocean dynamics are shown to be barotropic wind-driven setup of sea level. The wind forcing, sea level and circulation patterns are also shown to be related to the MJO and this relationship is shown to vary with season and wind direction. A strong seasonality in the sea level variations is found which is related to the seasonal variation of the MJO-wind relationship. It should be noted that this paper shares many of the goals and methodology as Oliver and Thompson (2011) and should be viewed as a companion study to that one.

This paper is organized as follows. The observations and reanalysis output are described in Sect. 2 and a statistical analysis of their variability is presented in Sect. 3. The ocean circulation model is described in Sect. 4 and is used in Sect. 5 to examine the dynamics of sea level and circulation in the Gulf of Thailand and the role of the MJO. A discussion of the results and our conclusions are presented in Sect. 6.

2 The MJO index and observations of sea level and surface wind

Seven hourly sea level records were obtained from tide gauges located around the Gulf of Thailand (Fig. 1) for

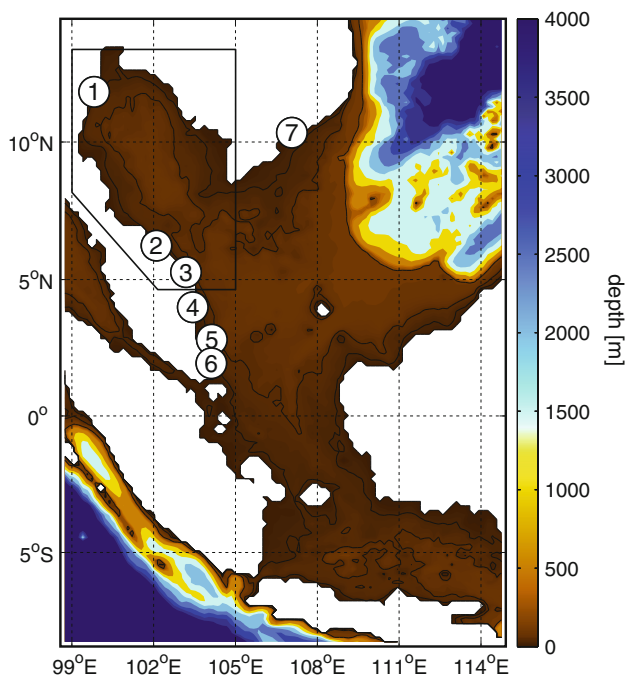


Fig. 1 The model domain and bathymetry. The 25, 50, and 200 m depth contours are indicated by black lines. The white circles show the tide gauge locations: (1) Ko Lak, (2) Geting, (3) Cendering, (4) Kuantan, (5) Tioman, (6) Sidili, and (7) Vung Tau. The black box over the Gulf of Thailand encloses the area used to calculate the Gulf-mean wind

the period 23/13/1983 to 30/12/2010. Details of individual record length, location and completeness can be found in Table 1. Tides were removed using the tidal analysis package of Pawlowicz et al. (2002) with 66 tidal constituents and then averaged to daily values using a Doodson X0 filter (Doodson 1928). Daily sea level pressures from the NCEP Climate Forecast System Reanalysis (CFSR, Saha et al. 2010) defined on a 1/2° grid were used to remove the inverse barometer effect. The annual cycle and its first two harmonics were removed using least squares prior to analysis. The daily mean residual is denoted by η_0 and sample plots of the time series are shown in Fig. 2.

Fields of surface (10 m) winds were obtained from CFSR (Saha et al. 2010) for the period 1/1/1979 to

31/3/2011 and the Climate Forecast System Reforecast version 2 (CFSv2, Saha et al. 2012) for the period 1/4/2011 to 31/12/2011. The CFSR data are defined on a global T382 Gaussian grid with an approximate horizontal resolution of 38 km; the CFSv2 data are defined on a global T575 Gaussian grid with an approximate horizontal resolution of 27 km. The wind fields were mapped onto the ocean model grid (described in Sect. 4) using a two-dimensional bicubic interpolation and the air-sea drag coefficient of Large and Pond (1981) was then used to calculate stresses. We define the “Gulf-mean wind” as the average over the area shown by the box in Fig. 1 (only data over ocean grid cells are included).

The MJO is characterized using the daily bimodal index of Wheeler and Hendon (2004) for the period from 1/1/1979 to 31/12/2011. This index consists of two time series which are based on the first two principal components calculated from tropical fields of observed outgoing long wave radiation and reanalysed zonal winds. This pair of time series describes an oscillating phenomenon which propagates eastward along the equator. Most of the energy of the MJO index lies in the 30–90 day band (power spectrum is shown in Fig. 3, shaded region; see “Appendix” for details on the calculation of the power spectrum). When the second component of the time series is plotted against the first component they form “MJO phase space” from which we can derive the instantaneous MJO amplitude and phase. If the amplitude of the MJO index is greater than 1 one it is assigned a particular phase (an integer between 1 and 8), corresponding to 45° divisions of MJO phase space, otherwise it is considered null (Wheeler and Hendon 2004).

3 Intraseasonal variability in observed sea level and surface wind

The annual cycle of η_0 was estimated for each tide gauge location by regression onto sinusoidal and cosinusoidal functions with an oscillation period of one year. Annual maxima of 15–25 cm are found with similar phases across all stations (peak in late December and early January, not

Table 1 Details on the tide gauge records

Tide Gauge	Latitude (N)	Longitude (E)	Start	End	% Complete
Ko Lak	11°48'	99°49'	2/1/1985	30/12/2010	94.9
Geting	6°14'	102°6'	17/12/1986	30/12/2006	99.0
Cendering	5°16'	103°11'	2/11/1984	30/12/2006	99.0
Kuantan	3°59'	103°26'	23/12/1983	30/12/2006	98.6
Tioman	2°48'	104°8'	14/11/1985	30/12/2006	97.1
Sidili	1°56'	104°7'	24/12/1986	30/12/2006	98.1
Vung Tau	10°20'	107°4'	2/1/1986	30/12/2002	97.1

The data were obtained from the Hawai'i Sea Level Center

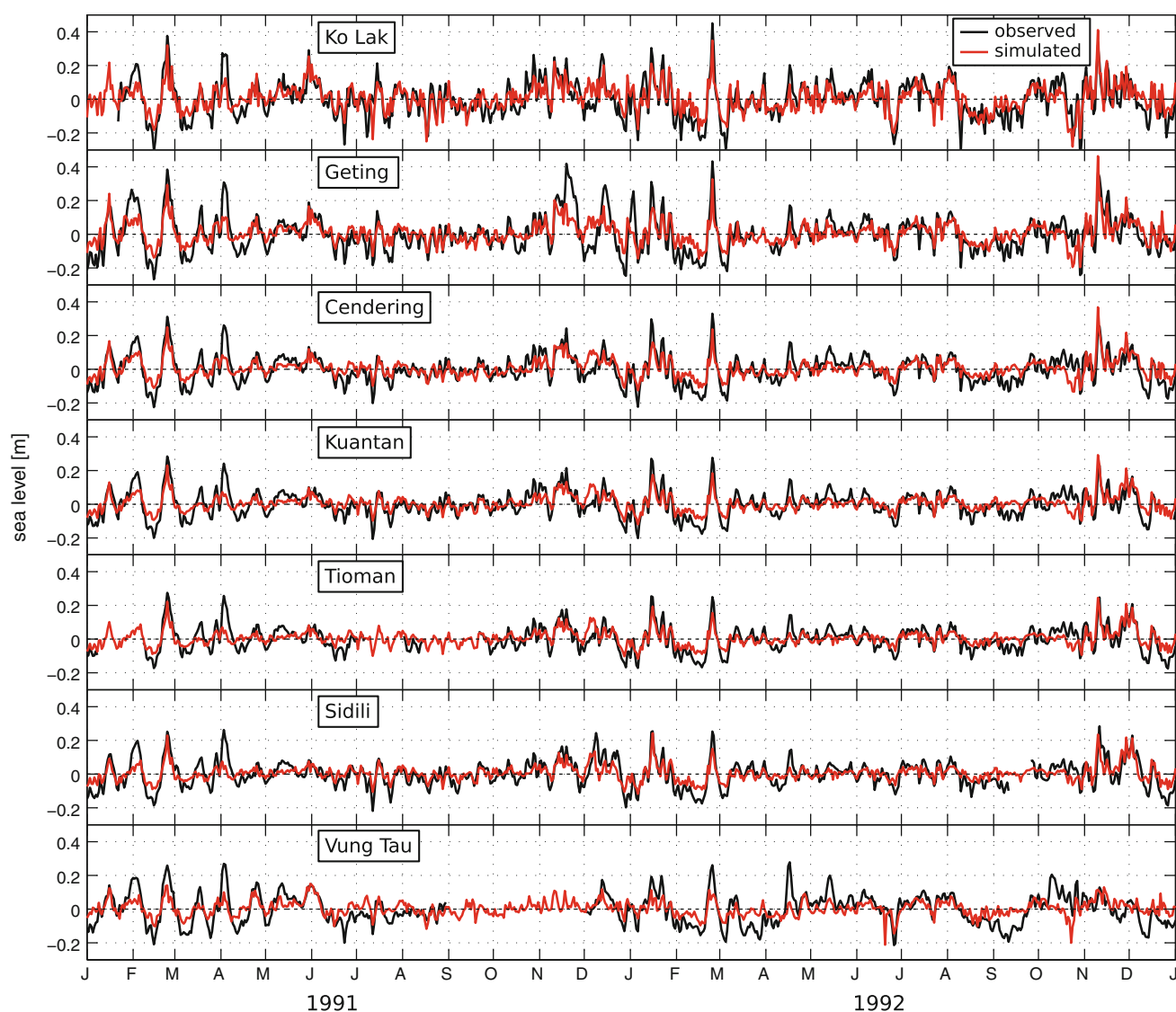


Fig. 2 Observed and simulated sea level over a typical 2-year period for (from top to bottom) Ko Lak, Geting, Cendering, Kuantan, Tioman, Sidili, and Vung Tau. The solid lines show the observed sea

level (η_o) and the red lines show the model simulation from the nearest wet grid cell (η_m). The series have been high-pass filtered with a cutoff period of 1/2-year

shown), consistent with Shaw and Chau (1994). The annual cycle (and its first two harmonics) were removed for the remainder of the analysis.

Power spectra of sea level in the Gulf of Thailand show peaks on intraseasonal time scales especially for Ko Lak and Geting which are near the head of the Gulf (Fig. 3, upper left). Variability in these time scales is also related to the MJO: the coherence between sea level at Ko Lak and the MJO is statistically significant and greater than ~ 0.5 over time scales where the MJO is most energetic (Fig. 4). (When we refer to the coherence between a scalar time series, such as sea level, and a bivariate time series, such as the MJO index, we mean the multiple coherence between the scalar time series and the two components of the bivariate time series, see “Appendix” for more

details.) The coherence is lower for the other stations (0.25–0.4) but most show a distinct local maximum on intraseasonal time scales. This suggests that the MJO may play an important role in intraseasonal sea level variability in the Gulf.

In order to further examine the role of the MJO on sea level variability we have calculated composites of sea level with the MJO phase. These composites show that the MJO modulates sea level in the Gulf with amplitudes of up to 4 cm at Ko Lak (Fig. 5, black lines) which are statistically significant at the 5 % level. The statistical significance of these composites was calculated using the Monte Carlo technique whereby the MJO phase vector is randomly shifted relative to the sea level series and the composites are recomputed (see Wheeler et al. 2009). This was done

Fig. 3 Relationship between the observed (η_o) and simulated (η_m) sea level in the Gulf of Thailand at the seven tide gauge locations. **a, d** Show the power spectral density of η_o and η_m respectively. **b** Shows the coherence between η_o and η_m and **c** shows the associated phase spectra. The shaded area indicates the total power of the MJO index (with power indicated on the right side of the **d**). The horizontal dashed line in the upper right panel indicates the 5 % significance level. The vertical dashed lines indicate periods of 30, 60 and 90 days (3.33×10^{-2} cpd, 1.67×10^{-2} cpd and 1.11×10^{-2} cpd respectively)

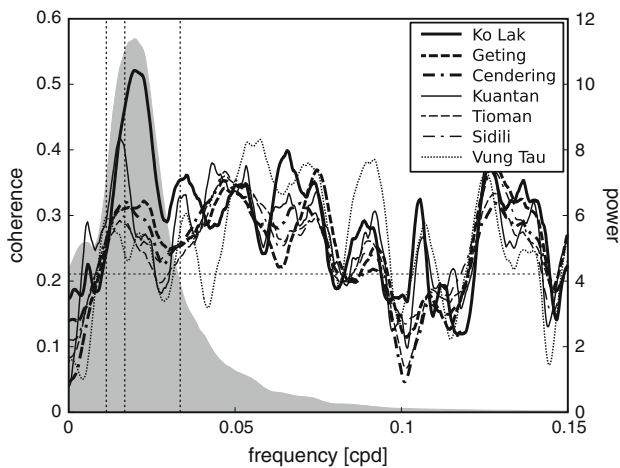
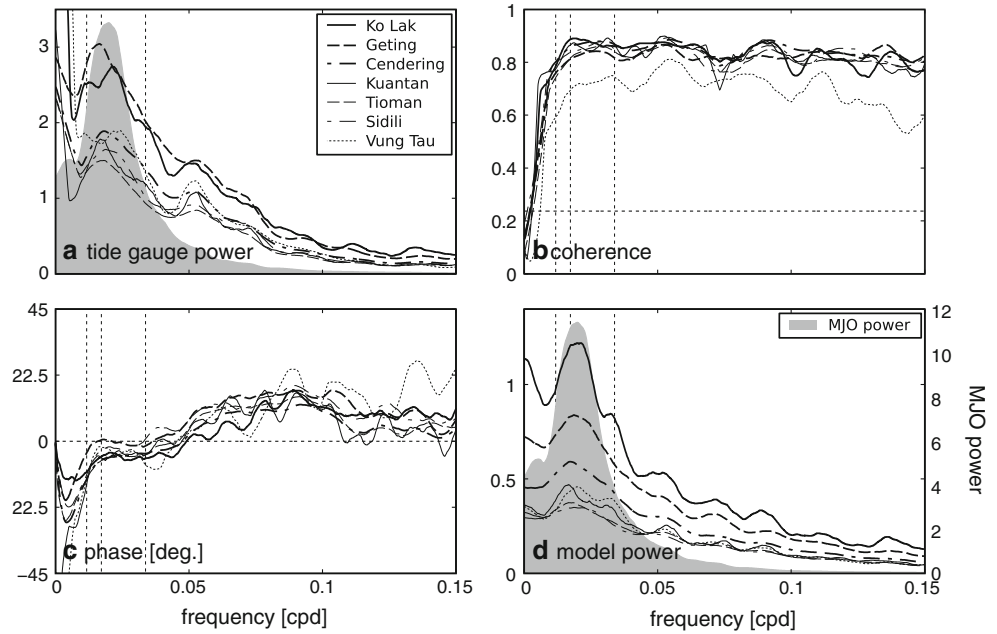


Fig. 4 Relationship between observed sea level and the Madden-Julian Oscillation. For each tide gauge (indicated by different line types) the multiple coherence is calculated with the MJO index. The shaded area indicates the total power of the MJO index (with scale shown on right edge of panel). The horizontal dashed line indicates the 5 % significance level for coherence. The vertical dashed lines indicate periods of 30, 60 and 90 days (3.33×10^{-2} cpd, 1.67×10^{-2} cpd and 1.11×10^{-2} cpd respectively)

1,000 times and the 95 % confidence interval is shown by the error bars in Fig. 5.

The relationship between sea level and the MJO may be a setup and setdown response to surface wind stress as suggested by Zhuang et al. (2010) and similar to the relationship shown to exist in the Gulf of Carpentaria by Oliver and Thompson (2011). The Gulf-mean wind is highly coherent (>0.7) with sea level variability at the tide gauges on time scales shorter than 1 year (Fig. 6, left panel). Furthermore, the Gulf-mean wind is strongly related to the

MJO, particularly the zonal component (coherence 0.7–0.8 over the time scales where the MJO is most energetic, Fig. 6, right panel). This evidence strongly supports the hypothesis that sea level variability in the Gulf is driven by MJO-related surface wind.

The surface wind variability over the Gulf of Thailand is also strongly linked to the local monsoon cycle. The northeasterly trade winds (also called the northeasterly monsoon) dominate over the November to March period. Over the April to September period the Asian monsoon causes a reversal of the mean flow with surface winds predominantly southwesterly. Wind strength is particularly weak during the pre-monsoon (March to May) and during the transition between the two monsoon regimes (October). The distribution of wind directions on intraseasonal time scales was estimated using a histogram. The full circle of angular directions was divided into 30 bins (the width of each bin was approximately 12°) and the average wind direction within each bin was then calculated. On intraseasonal time scales the wind anomalies are predominantly in the easterly/westerly direction (see Fig. 7, histogram bars; the tallest bar represents a total of 714 days at that wind direction).

To examine the relationship between the MJO and Gulf-mean wind direction we calculated the direction-dependent intraseasonal coherence. The coherence was calculated between the Gulf-mean wind, projected onto an axis, and the MJO index. These coherencies were then averaged over intraseasonal time scales (between 30 and 90 days) and plotted as a function of 360 discrete axis directions covering a full circle (Fig. 7, solid line). The intraseasonally-averaged coherence with the MJO is greatest for wind

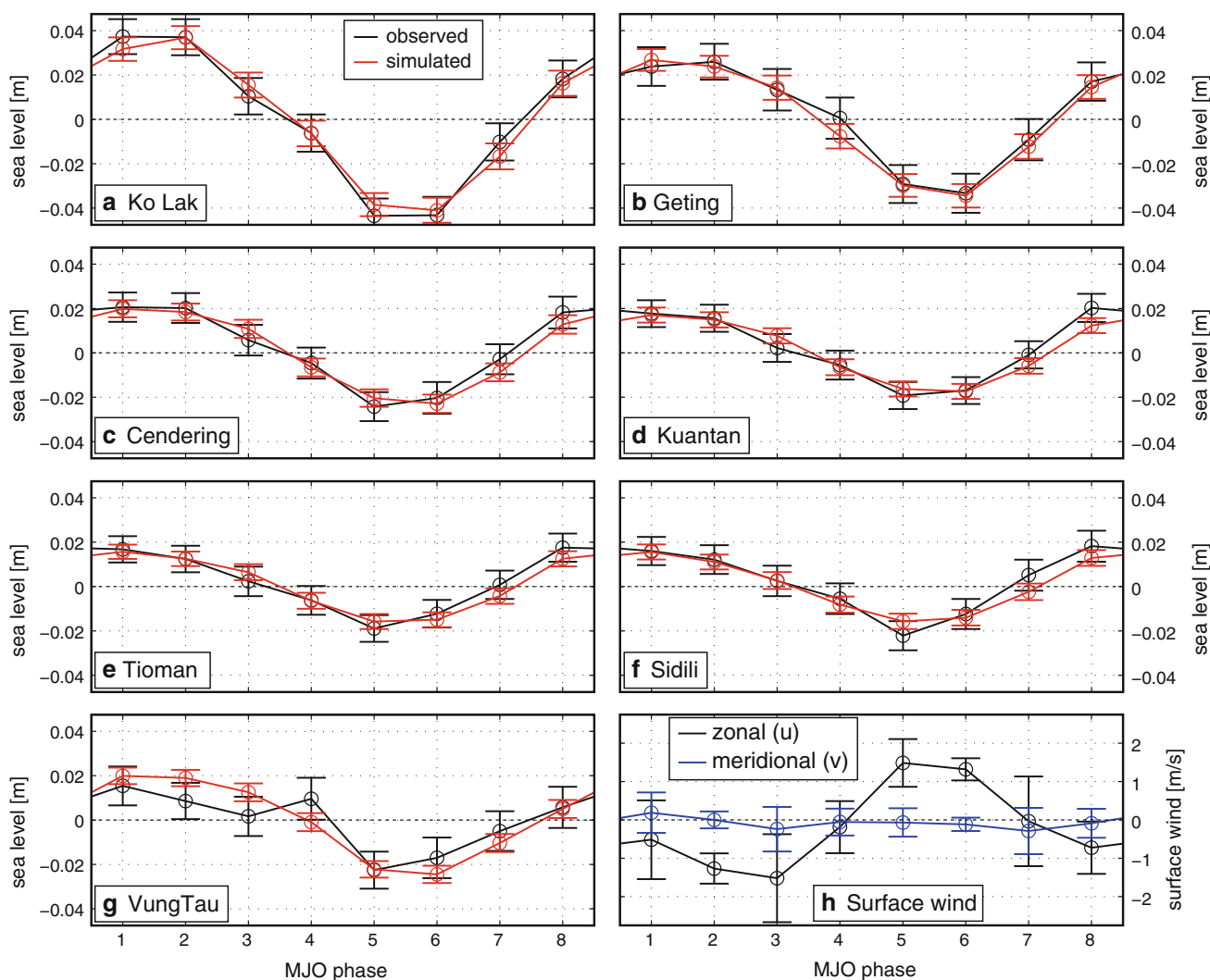


Fig. 5 Relationship between the MJO and sea level at the tide gauge locations and surface wind. **a–g** Composites of η_o (black lines) and η_m (red lines) with the MJO index. **h** Composites of zonal (black) and

meridional (blue) surface wind over the Gulf of Thailand with the MJO index. Error bars indicate the 95 % confidence intervals

directions ranging from westerly to northwesterly (or equivalently easterly to southeasterly since we are considering intraseasonal anomalies). The direction for peak relationship with the MJO corresponds to the direction of predominant wind variability on intraseasonal timescales (Fig. 7, histogram bars). We will show in Sect. 4.2 that sea level in the the Gulf of Thailand responds most strongly to winds approximately in this direction as well. Therefore, it is anticipated that the MJO will provide a strong contribution to intraseasonal wind-driven sea level variability (and associated circulation variability) in the Gulf.

Another way of exploring the relationship between the MJO and Gulf-mean wind is by compositing based on MJO phase. On intraseasonal time scales, anomalous easterlies are experienced over the Gulf when the convective anomaly associated with the MJO propagates from the Indian ocean eastward onto the Maritime Continent (phases

1–3); anomalous westerlies are experienced over the Gulf when this convective anomaly moves into the Western Pacific (phases 5–6, Fig. 5h, black line). This is consistent with the behaviour of coastal sea level which exhibits peak setup during phases 1–2 and peak setdown during phases 5–6 across all stations (Fig. 5a–g). The meridional component of the surface wind is not significantly different from zero during any MJO phase (Fig. 5h, blue line).

In addition to the mean wind, the wind variability is also strongly seasonal. The seasonal cycle of wind variability and its relationship with the MJO was examined by calculating seasonally stratified power spectra of the zonal component of the Gulf-mean wind (see “Appendix” for details on this calculation). Figure 8 shows that on intraseasonal time scales the zonal wind is very energetic from June to February (left panel). This period of time also corresponds to when the zonal wind is most coherent with

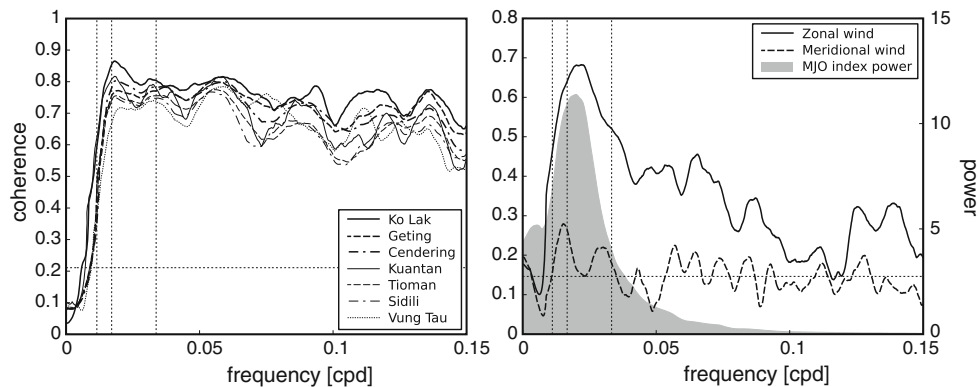


Fig. 6 Relationship between the surface wind over the Gulf of Thailand and sea level variability (*left*) and the MJO (*right*). The *left panel* shows the coherence between η_0 and both components of the Gulf-mean wind. The *right panel* shows the coherence between the MJO index and the zonal (*solid*) and meridional (*dashed*) components of the Gulf-mean wind. The *shaded area* indicates the total power of

the MJO index (with scale shown on *right edge of panel*). The *horizontal dashed lines* indicate the 5 % significance level. The *vertical dashed lines* indicate periods of 30, 60 and 90 days (3.33×10^{-2} cpd, 1.67×10^{-2} cpd and 1.11×10^{-2} cpd respectively)

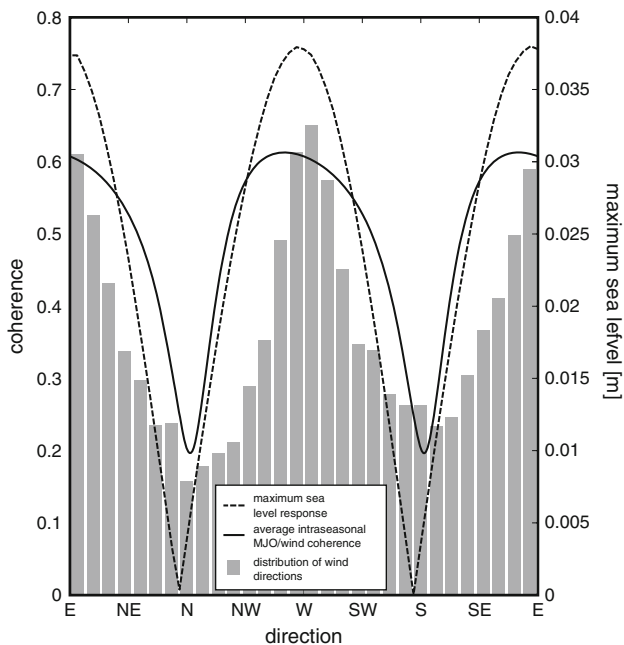


Fig. 7 Wind direction and its relationship to sea level in the Gulf of Thailand and the Madden–Julian Oscillation. A histogram of daily Gulf-mean wind directions is shown by the *grey bars*. (The wind series has been deseasonalized prior to the calculation of wind direction.) The coherence, averaged over the 30–90 day band, between the Gulf-mean wind projected onto the direction indicated and the MJO is shown by the *solid line*. The steady-state response of sea level in the Gulf, simulated by the numerical model, to uniform wind forcing as a function of wind direction is shown by the *dashed line*

the MJO index (0.75–0.9, right panel). The intraseasonal variability and the MJO-wind coherence are weakest during the pre-monsoon (March–May) when the mean wind is weakest; the intraseasonal variability is strong in October during the transition between the two monsoon regimes

indicating that the variance remains large despite a reduced mean wind speed. The seasonal timing is also consistent with the seasonal cycle of observed intraseasonal precipitation variability in this region (Hsu 2012).

The seasonal cycle of observed sea level variability was calculated in the same way as for the wind and shows a similar cycle (Figs. 9, 10, left panels). This is especially true at Ko Lak which is nearest to the head of the Gulf. We will use the circulation model (described in the next section) to reproduce these sea level variations and then use it to map the sea level and circulation response to the MJO over the entire Gulf of Thailand.

4 Numerical model

The numerical ocean model used to simulate the Gulf of Thailand and immediately adjacent shallow regions was the fully nonlinear Princeton Ocean Model (POM, e.g. Blumberg and Mellor 1987). The model configuration is described (Sect. 4.1) followed by process studies which to describe potential natural resonances in the Gulf (Sect. 4.2)

4.1 Model configuration

The model configuration was similar to that used by Oliver and Thompson (2011) but with important differences outlined here. The model domain is shown in Fig. 1. The model variables are arranged on an Arakawa C-grid with a spatial resolution of $1/6^\circ$ (138 points latitudinally and 99 points longitudinally). The bathymetry (Fig. 1) was averaged onto to the model grid from the high-resolution (30 arc-second) General Bathymetric Chart of the Oceans (IOC et al. 2003). The surface wind was derived from six-hour

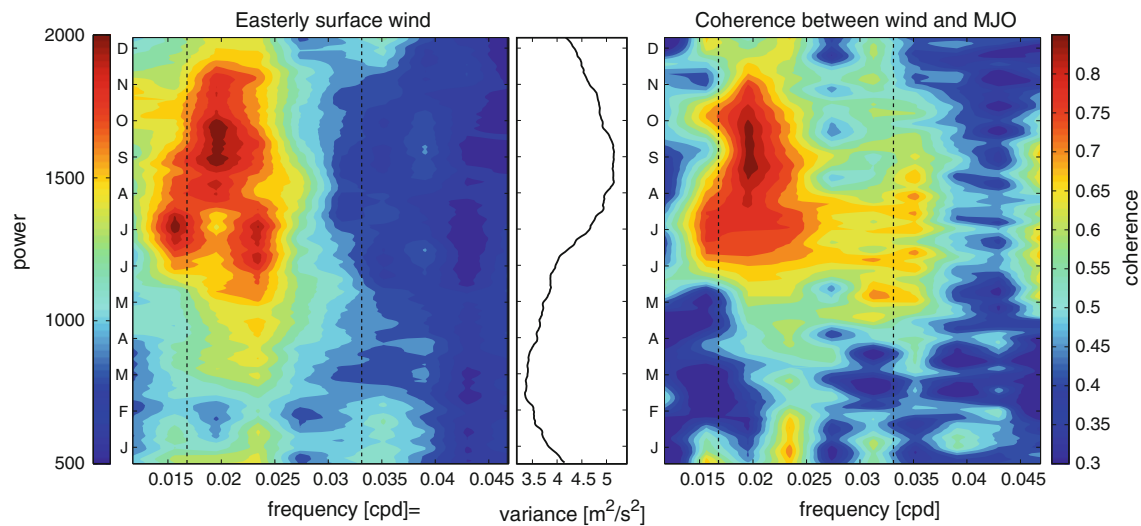


Fig. 8 Seasonal cycle of the zonal Gulf-mean wind variability and its relationship to the MJO. *Left panel* the seasonal cycle of the spectral density of zonal wind over the intraseasonal band. The spectrum for a particular time of year has been normalized by the total variance at that time of year (*middle panel*) in order to emphasize the seasonal

changes in spectral shape. *Right panel* the seasonal cycle of the coherence between zonal wind and the MJO index over the intraseasonal band. The *dashed lines* indicate periods of 30 and 60 days (3.33×10^{-2} cpd and 1.67×10^{-2} cpd respectively)

CFSR and CFSv2 reanalysis surface winds, linearly interpolated to the model time step, and was used to force the model. Note that the effect of atmospheric pressure variations was ignored.

The model was run in two-dimensional barotropic mode with the density of water fixed at 1025 g kg^{-1} . The boundary condition at the coasts was no normal flow and no slip; at the open boundaries radiation conditions were applied to allow waves generated within the domain to escape. The bottom stress was of the form $c_d \mathbf{u}|\mathbf{u}|$ where the minimum and maximum values of the bottom friction coefficient c_d were 2.5×10^{-3} and 5×10^{-3} , respectively, and \mathbf{u} is depth averaged flow. The initial condition was zero flow and a flat sea surface. The time step for the calculation was 12 s. The model was run for 1979–2011 (33 years) and depth-averaged sea level and current fields were output daily.

4.2 Natural resonances

Natural resonances in the Gulf due to wind direction or period of oscillation may confound the analysis of the response to MJO-related forcing so they must be ruled out before proceeding further. To test for a natural resonance of the Gulf on intraseasonal time scales the model was forced by periodic easterly/westerly winds with an amplitude of 10 m s^{-1} for 700 days. Runs were performed for forcing with oscillation periods between 5 and 150 days. Sea level was averaged spatially over the domain bounded by 99.1°E , 101.9°E , 8.1°N , and 14.4°N and a steady oscillation of average sea level in this domain takes

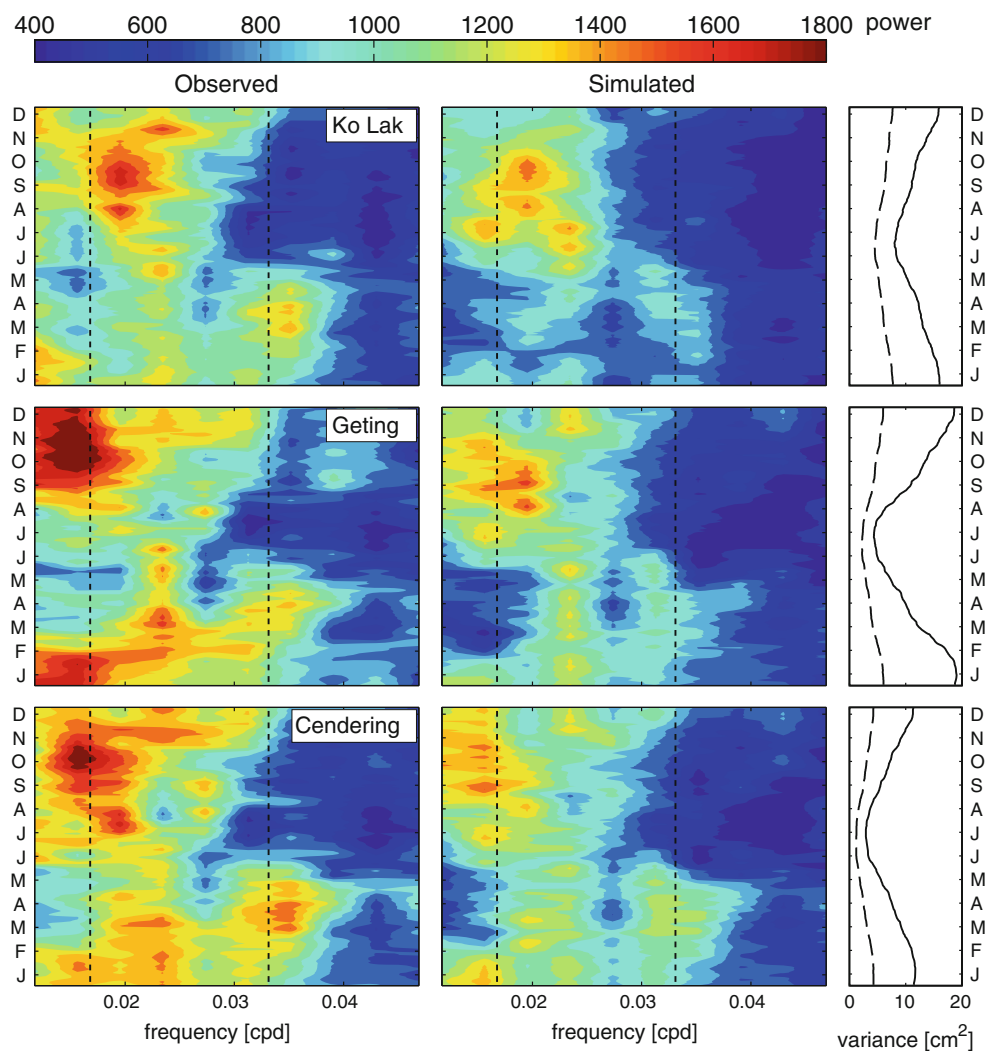
approximately 10 days to spin up. The maximum amplitude (gain) over the final 350 days was calculated for each run and plotted against the oscillation period of the forcing (not shown). Over the intraseasonal band (30–90 days) the gain deviates by less than 4 % from a flat line; there is a peak in the gain for oscillation periods of 8 days but this may be due to aliasing of the daily time series. Therefore, we can rule out the possibility of a natural resonance on intraseasonal time scales.

The dependence of sea level setup on wind direction was examined in a second set of sensitivity studies. Sixty-four separate model simulations were performed with a wind forcing speed of 5 m s^{-1} at 64 discrete wind directions. The steady state response was averaged over the same spatial domain defined above and days 201–365 of the model output. The largest setup (setdown) response of sea level was found for westerly (easterly) winds (dashed line, Fig. 7b), consistent with the discussion in Sect. 3

5 Model simulated sea level and comparison with observations

The sea level simulated by the ocean model for the 1/1/1979 to 31/12/2011 period was used to examine the influence of the wind, and thus the MJO, on coastal sea level in the Gulf of Thailand. A comparison of the model simulations to the observed coastal sea level is performed first (Sect. 5.1). The response of sea level and circulation in the Gulf to the MJO is then mapped (Sect. 5.2) followed by an exploration of its potential predictability (Sect. 5.3)

Fig. 9 Seasonal cycle of observed and simulated sea level variability at Ko Lak (top row), Geting (middle row), and Cendering (bottom row). Left panels correspond to observations and middle panels to model simulations. The spectra have been normalized by the variances shown in the right panels (solid observations, dashed simulations). Otherwise same format as Fig. 8



5.1 Validation of simulated sea level

The annual cycle of the simulated sea level was estimated for each tide gauge location as in Sect. 3. The simulated annual cycles are generally smaller in amplitude ($\sim 5\text{--}10$ cm) than the observed annual cycles and the simulated peak amplitude is reached 1–2 months later than for the observations (not shown). Steric sea level changes, those due to thermal expansion and salinity variations in the neighbouring deep waters and which are present in the observations and not in the model simulations, may account for this difference.

The annual cycle (and its first two harmonics) were then removed from the model simulations of sea level at each tide gauge location and the residuals are denoted η_m . The model captures the observed intraseasonal variability well (time series can be seen in Fig. 2, red lines). The observed and simulated time series, filtered to remove variability on time scales longer than 1/2-year, are well-correlated (0.63–0.79, see Table 2). In terms of standard deviation, the model simulations underestimate the observed time series and the

standard deviation of the difference is generally similar to that of the model simulations (see Table 2). The model simulations capture the spectral peak on intraseasonal time scales (Fig. 3, compare upper left and lower right panels). The coherence over these time scales is high (0.7–0.9, Fig. 3, upper right panel) with phase lags near zero (Fig. 3, lower left panel, see “Appendix” for details on the phase spectrum).

The model simulations have a similar seasonal cycle of intraseasonal variability (Figs. 9, 10). As with the annual cycle, the model underestimates the amplitude of the observed variability. However, the fact that η_o and η_m are well-correlated and exhibit the same seasonal cycle of variability indicates that the model captures the important aspects of the wind-driven response, particularly the timing, of the Gulf of Thailand on intraseasonal timescales.

5.2 Influence of the MJO on circulation and sea level

Composites of η_m with MJO phase were calculated in order to examine the relationship between the MJO and sea

Fig. 10 Seasonal cycle of observed and simulated sea level variability at Kuantan (*top row*), Tioman (*middle row*), and Sidili (*bottom row*). Same format as Fig. 9

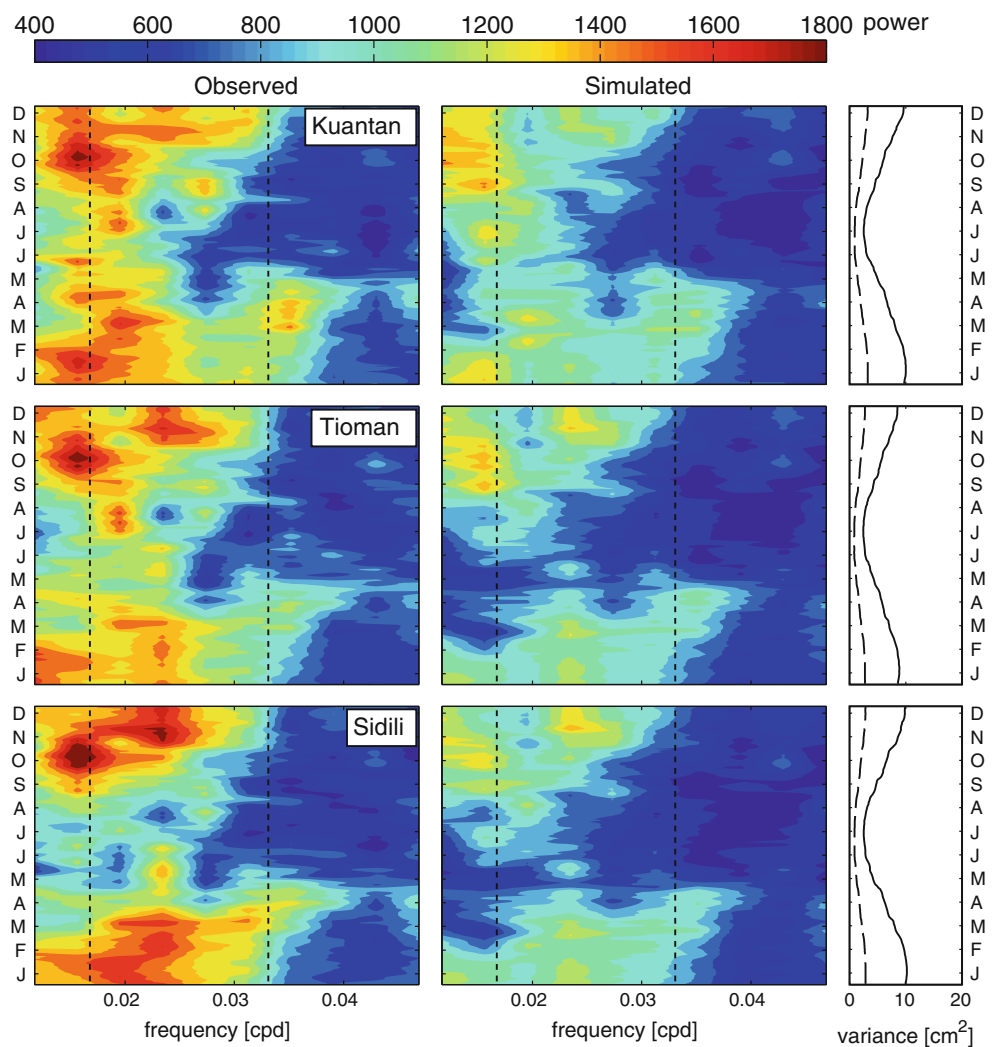


Table 2 Comparison of observed and simulated sea level

Name	σ_o (cm)	σ_m (cm)	σ_{o-m} (cm)	ρ_{om}
Ko Lak	10.92	7.79	7.26	0.748
Geting	10.84	6.47	7.27	0.760
Cendering	8.79	5.29	5.62	0.791
Kuantan	8.06	4.62	5.32	0.779
Tioman	7.72	4.39	5.25	0.758
Sidili	8.13	4.38	5.52	0.770
Vung Tau	8.76	4.53	6.89	0.629

The columns (from left to right) are the standard deviation of the observed (σ_o) and simulated (σ_m) sea level, the standard deviation of their difference (σ_{o-m}), and the correlation (ρ_{om}) between them (standard deviations are in cm). A highpass-filter with a cutoff period of 1/2-year was applied to the observed and simulated sea level series

level and circulation in the Gulf of Thailand. Composites of η_m at the tide gauge locations agree well with observations in terms of timing and amplitude (Fig. 5a–g, red lines). The role of the MJO on sea level and circulation in

the entire Gulf of Thailand can be examined by extending the composite analysis to the entire model domain. These maps show that the Gulf goes through a cycle of sea level setup (phases 8 and 1–3) and setdown (phases 4–7) as the Gulf-mean wind oscillates from easterlies to westerlies (Fig. 11, coloured contours). The sea level response is particularly strong along the western side of the Gulf and appears to extend all along the Malay Peninsula.

The circulation anomalies are generally anticyclonic during the setup phases (e.g., phase 3) and cyclonic during the setdown phases (e.g., phase 7, Fig. 11, black arrows). At peak setup and setdown there is very strong flow (up to 10 cm s^{-1}) along both sides of the mouth of the Gulf of Thailand (Cape of Camau to the northeast and mainland Malaysia to the southwest). There is also strong flow through the Malacca Strait out of (in to) the South China Sea during setup (setdown). Therefore, the influence of the MJO is not just at the coast, as indicated by the tide gauges, but significant sea level and circulation variations extend over the entire Gulf and adjacent regions.

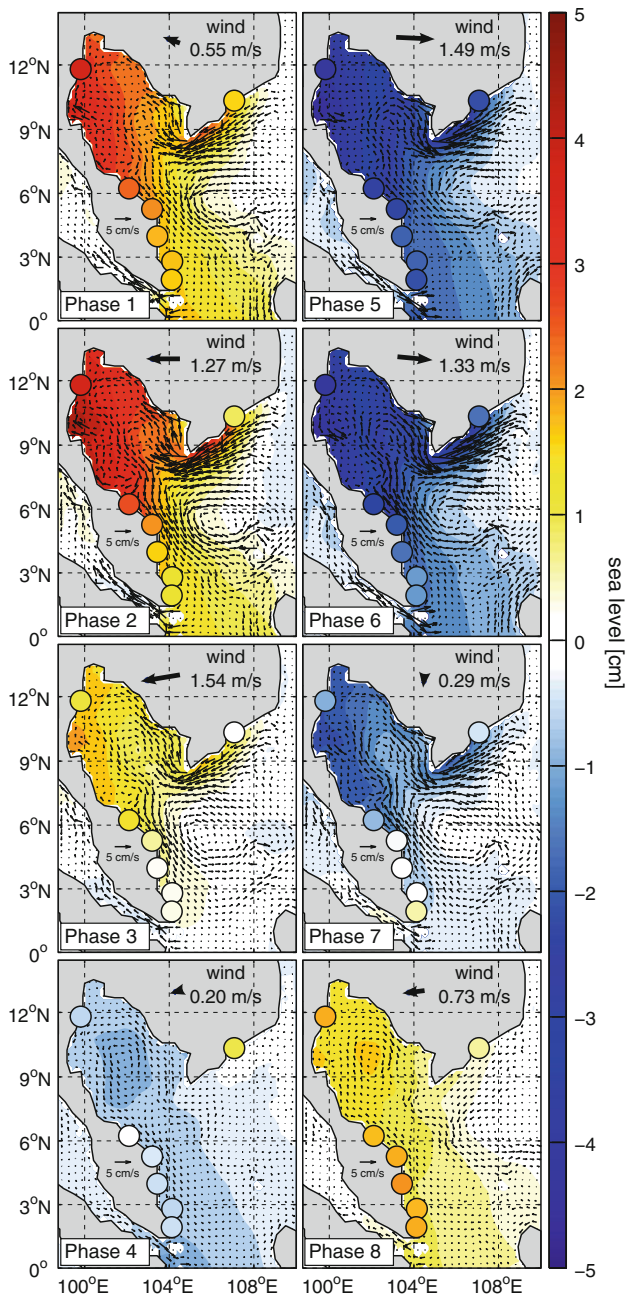


Fig. 11 Composites of sea level, depth-averaged current anomalies, and surface wind associated with phases 1 through 8 of the MJO (top to bottom, left to right). The thick arrows near the top of each panel are the composites of the Gulf-mean wind with the wind speed indicated next to the arrow. The filled contours show the composites of modeled (η_m) and observed (η_o) sea level, respectively, and the black arrows show composites of model simulated currents. A reference arrow of 5 cm s^{-1} is located on the Malay Peninsula in each panel

5.3 Potential predictability

The potential predictability of sea level setup in the Gulf, and by extension the associated circulation pattern, is

explored by comparing time series of sea level from Ko Lak to the MJO index over the 1996–2001 period (Fig. 12). Intraseasonal variability of η_o and η_m agree very well over this time period (Fig. 12, black and red lines respectively). The intraseasonal sea level variability also agrees well with the MJO index which is shown projected onto the phase 1/phase 5 axis, with positive values representing phase 1 (this axis was chosen based on the composite maps shown in Fig. 11). The good correspondence between the timing of sea level and MJO events is particularly true during Boreal Summer, Fall, and Winter (June to February); the correspondence tends to break down during Boreal Spring (March to May) which is when the intraseasonal wind variability is weakest (Fig. 8, left panel). The correspondence also tends to be weaker between June of 1998 and February of 1999 suggesting a possible link to ENSO activity (e.g., due to the large 1997/1998 El Niño event). However, composites of η_o based on the eight phases of the MJO did not show a statistically significant difference in the MJO/sea level relationship during El Niño, La Niña, and null years (defined based on the NINO3.4 index; not shown).

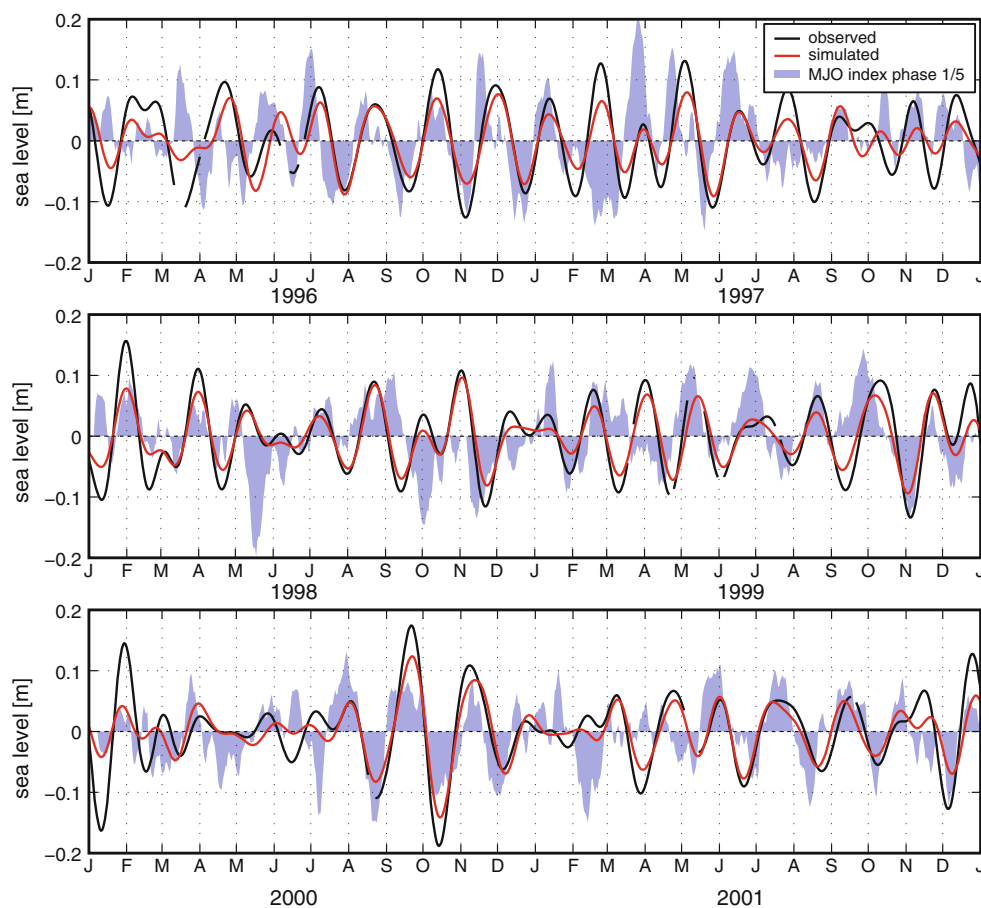
The potential predictability of the MJO-related sea level setup in the Gulf of Thailand can be quantified using a simple statistical prediction model. We relate the observed Ko Lak sea level series (η_t) and the MJO index (first and second components: $I_{1,t}$ and $I_{2,t}$) using a lagged linear regression model

$$\eta_{t+k} = \sum_{d=0}^D \beta_{1,d} I_{1,t-d} + \beta_{2,d} I_{2,t-d} + \epsilon_t, \quad (1)$$

where t is a time index, k is a future prediction time, the β are regression coefficients and ϵ_t is an error term. The model includes $I_{1,t-d}$ and $I_{2,t-d}$ at all lags d from 0 to D . In practice the inclusion of so many lags provides an overfit model and in this study we only include lags 0, 15 and 30 days which, after experimenting with many combinations, were found to provide consistent high correlation values.

The model is trained on the first half of the time period (2/1/1985–31/12/1997, ~ 8 years) and validation statistics are calculated over the second half of the period (1/1/1998–30/12/2010, ~ 8 years). The model is trained over July through January only (the period where the MJO-sea level connection is strongest) for each year in the training period and for points in time for which the MJO amplitude is greater than 1. Extra tests were performed where the training period was further restricted based on an increasing or decreasing MJO amplitude, defined as an positive or negative difference in MJO amplitudes over a two-day period. The record is not continuous over the training period but is discrete due to these seasonal- and

Fig. 12 Predictability of sea level setup in the Gulf of Thailand. Time series of η_o and η_m at Ko Lak for 1996–2001, after bandpass filtering in the 30–90 day band, are shown by the *black* and *red lines*, respectively. The MJO index, projected onto the phase 1/phase 5 axis (with positive values representing phase 1) is shown by the *light blue shading*



MJO-based restrictions. The time points were restricted over the validation period in the same way.

The correlation of the model simulations and η_t (over the validation period) as a function of future prediction time k is shown in Fig. 13 (solid line). The correlation is approximately 0.32 instantaneously ($k = 0$ days). The correlation at future prediction times are similar up until $k = 5$ days at which point it begins to decrease reaching zero at about $k = 14$ days. However, after 10 days the correlation only drops by half indicating that in this time period the model can still account for some (5–10 %) of the variability. (These correlation values may seem low but it should be kept in mind that, in order to simulate a real-time prediction system, the sea level record was not filtered and so retains variability on time scales outside the intraseasonal band.) The model was also fit for periods of time when the MJO amplitude was increasing or decreasing corresponding to a growing or diminishing MJO event (Fig. 13, dashed and dot-dashed lines respectively). The model provides enhanced predictability out to about 8 days when the MJO amplitude is increasing and decreased predictability when the MJO amplitude is decreasing.

6 Summary and discussion

Observational records from tide gauges, reanalyzed surface wind and a barotropic ocean circulation model were used to show that a significant component of intraseasonal sea level variability in the Gulf of Thailand is driven by MJO-related wind stress. An initial statistical analysis of observed sea level and reanalyzed wind variability indicated that the sea level variability was consistent with seasonal changes in zonal surface wind variability and that this wind variability was strongly related to the MJO. The ocean model, which was validated against the observed sea level, was then used to map the MJO-related sea level pattern in the entire Gulf of Thailand as well as the associated depth-averaged circulation.

Sea level from seven tide gauges in the Gulf of Thailand were shown to have a moderate relationship with the MJO, strongest at the head of the Gulf. It was also shown that sea level variability on time scales shorter than one year was highly coherent with surface wind variability, i.e., on these time scales the sea level variability is strongly linked to wind stress variability. Additionally, the seasonal cycles of intraseasonal sea level and zonal wind variability had the

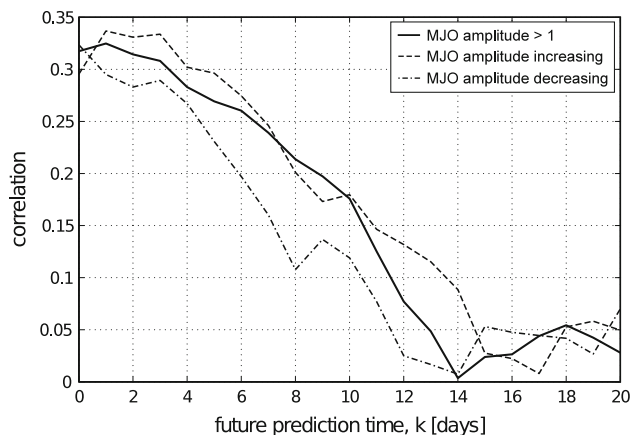


Fig. 13 Potential predictability of sea level variability at Ko Lak from the MJO. The correlation between the lagged regression model (with lags 0, 15 and 31 days) and Ko Lak sea level over the validation period is plotted as function of future prediction time k (solid line). The results for the model applied only for increasing MJO amplitude and decreasing MJO amplitude are shown as dashed and dot-dashed lines respectively

same structure, being strongest during the monsoon seasons (June through February). Finally, the Madden–Julian Oscillation was strongly linked to this variability except during March to May when the surface wind makes the transition between the trade winds and the monsoon-dominated winds. Therefore, the observational evidence indicated that intraseasonal sea level variability was partially driven by MJO-related wind forcing.

The wind-driven sea level and circulation variability in the Gulf was reconstructed over the 1979–2011 period using a barotropic circulation model. The model was able to reproduce the intraseasonal sea level variability observed at the seven tide gauge locations with high correlation coefficients and coherencies on time scales shorter than about 1 year. The model was also able to reproduce the seasonal cycle of intraseasonal sea level variability.

The response of the Gulf of Thailand shows a predictable cyclic response to the MJO. As the convective region of the MJO propagates from the Indian Ocean eastwards to the Maritime Continent, easterly surface wind causes a setup of sea level of up to 5 cm and spins up an anticyclonic gyre in the Gulf (MJO phases 8 and 1–3); as the convective region propagates away from the Maritime Continent to the Western Pacific, westerly surface wind causes a setdown of sea level and spins up a cyclonic gyre in the Gulf (MJO phases 4–7). A simple statistical model demonstrates that the MJO index can account for 5–10 % of the sea level variability at the head of the Gulf of Thailand with a lead time of up to 10 days. This simple model uses the unfiltered sea level and MJO index time series and so provides an upper limit on real-time predictability of the Gulf of Thailand sea level response. Such

a statistical model may lead to more accurate predictions of intraseasonal sea level and circulation variability important for planning in coastal communities and possibly changes in biological productivity in the Gulf of Thailand.

A diagnostic three-dimensional model run was also performed to test the sensitivity of the Gulf of Thailand to seasonal stratification changes (not shown). Temperature and salinity were held fixed at climatological values derived from World Ocean Atlas 2009 seasonal climatologies (Antonov et al. 2010; Locarnini et al. 2010). The differences between correlations and coherence spectra of η_o and η_m from both runs were negligible, e.g., $O(0.05)$, and the timing of the seasonal cycle of the mean and the variability were essentially the same. Therefore, we can conclude that the intraseasonal variability of sea level, in terms of correlations and the timing of the seasonal cycle of variability, was not sensitive to seasonal changes in stratification.

It is possible that there may be significant intraseasonal sea level variability due to remotely-forced waves propagating into the Gulf of Thailand from the Indian or Pacific Oceans. To test this, first the average zonal and meridional surface wind in the equatorial western Pacific (140°E–160°E, 5°S–5°N) and the central Indian Ocean (70°E–90°E, 5°S–5°N) were calculated from daily CFSR 10 m wind fields. Sea level at Ko Lak was coherent with zonal wind over the Pacific Ocean on time scales of 40–65 days and with zonal wind over the Indian Ocean on time scales of 50–57 days (not shown; statistically significant at the 5 % significance level). Indian Ocean surface wind variability leads sea level by 10–20 days and Pacific Ocean surface wind variability lags sea level by 10–20 days over these time scales. However, the local MJO-related wind over the Gulf of Thailand should lag Indian Ocean wind variability by 1–2 MJO phases and lead Pacific Ocean wind variability by 1–2 MJO phases (Wheeler and Hendon 2004), consistent with the lead/lag relationship found between sea level and remote wind forcing. Therefore, it is not possible to determine for certain if these coherence and phase relationships are due to (1) the propagation of MJO-related wind anomalies from the Indian Ocean, over the Maritime Continent, and then the Pacific Ocean, or (2) ocean waves generated in the open ocean then propagating into the Gulf of Thailand region. Variability driven by remotely forced waves propagating into the domain is not likely, given that the numerical model (which includes only local forcing, i.e., no boundary forcing) reproduces well the intraseasonal variability in sea level, including the timing relative to the MJO. However a study covering a larger domain using a numerical model that permits the appropriate wave modes would be required to fully address this issue.

It is interesting to note that the Gulf of Thailand does not appear as a region of strong connection between sea level variability and the MJO in Oliver and Thompson (2010)

but does exhibit large and statistically significant anomalies in the composite maps of Webber et al. (2010). In Oliver and Thompson (2010), the map of MJO-related standard deviation of sea level (σ_p) was masked according to a constant, globally representative 5 % significance level. In this fashion, the sea level variability in the Gulf of Thailand appeared not to have a statistically significant relationship with the MJO. However, in principle the significance level is spatially varying. A map of σ_p , masked according to a 5 % significance level that has been calculated independently at each point in space, shows a statistically significant relationship between observed (AVISO) sea level variability in the upper part of the Gulf and the MJO (not shown). This calculation indicates that the MJO accounts for 30–35 % of the standard deviation (or 2–3 cm) in the upper Gulf consistent with the results in this paper.

Further research could examine the MJO-related sea level and circulation variability in the Indonesian Archipelago as a whole. This region is very shallow, particularly the western half adjacent to the islands of Borneo, Sumatra, and Java, and straddles the Equator where MJO-related wind forcing is strong. Therefore, we expect the ocean to exhibit a strong amplification of MJO-related wind forcing. However, patterns of MJO-related ocean variability may be quite different from what is found in shallow semi-enclosed seas such as the Gulf of Thailand and the Gulf of Carpentaria due to many points of open access to the deep ocean.

The analysis performed here only considers the Madden–Julian Oscillation as quantified by Wheeler and Hendon (2004). This index does not distinguish between the canonical eastward propagating Madden–Julian Oscillation, which is confined to lie approximately over the Equator, and the northwestward propagating Boreal Summer Intraseasonal Oscillation (BSISO) which occurs primarily over India, Southeast Asia, and East Asia. Recently, the BSISO has been quantified in a similar manner as the MJO index (i.e., Kikuchi et al. 2012; Lee et al. 2012) and it would be interesting to explore the relative roles played by the canonical MJO and the BSISO in driving intraseasonal variability in the Gulf of Thailand.

Acknowledgments ECJO would like to thank Bob Dattore at the University Corporation for Atmospheric Research (UCAR) for his assistance in obtaining the most recent Climate Forecast System Reanalysis and Reforecast (CFSR and CFSv2) output. ECJO would also like to thank Keith R. Thompson at Dalhousie University (Canada) for helpful comments and discussion. ECJO would also like to acknowledge the two anonymous reviewers for their critical and helpful comments.

Appendix: Spectral analysis

Consider two scalar random processes $\{x_t\}$ and $\{y_t\}$ where $t = 1, 2, \dots$ is a time index. The power spectra of $\{x_t\}$ and

$\{y_t\}$ are denoted $f_{xx}(\omega)$ and $f_{yy}(\omega)$, respectively, and their cross-spectrum is denoted $f_{xy}(\omega)$, where ω is the frequency. The power spectra and cross-spectrum are calculated from

$$f_{xy}(\omega) = \langle I_{xy}(\omega) \rangle \tag{2}$$

where $I_{xy}(\omega) = d_x(\omega)d_y^*(\omega)$ is the periodogram and $d_x(\omega)$ is the discrete Fourier transform of $\{x_t\}$ and is in general complex valued. The complex conjugate is denoted by $*$ and a weighted running average, in the frequency dimension, is denoted by $\langle \rangle$. The weighted running average is required because without performing such smoothing the periodogram does not provide a consistent estimator of the power spectra (e.g., Shumway and Stoffer 2000). An N -point Bartlett window, with N typically 10–20 % of the length of the original time series, is used in this study.

The squared coherence between $\{x_t\}$ and $\{y_t\}$ is defined by Priestley (1981)

$$\kappa_{xy}^2(\omega) = \frac{|f_{xy}(\omega)|^2}{f_{xx}(\omega)f_{yy}(\omega)}, \tag{3}$$

The coherence is confined to lie between 0 and 1 and can roughly be thought of as a “frequency-dependent correlation coefficient” (Eq. 3 is similar in form to the equation for squared correlation if the cross-spectrum is replaced by the cross-covariance and the power spectra are replaced by the auto-covariances). The associated phase spectrum $\phi_{xy}(\omega)$ is given by

$$\phi_{xy}(\omega) = \arctan\left(\frac{\text{Im}(f_{xy}(\omega))}{\text{Re}(f_{xy}(\omega))}\right) \tag{4}$$

where $\text{Re}(z)$ and $\text{Im}(z)$ represent the real and imaginary parts of z respectively. Given a statistically significant value of κ_{xy} at some frequency ω_0 then $\phi(\omega_0)$ represents the phase offset, in radians, between the coherent signals of $\{x_t\}$ and $\{y_t\}$ at the frequency ω_0 .

Given the bivariate random process $\{x_t\}$ where x_t is given by $[x_1 \ x_2]_t$ the coherence between $\{y_t\}$ and both components of $\{x_t\}$ can be calculated using the squared multiple coherence (Priestley 1981):

$$\kappa_{xy}^2(\omega) = \frac{f_{xy}(\omega)f_{xx}^{-1}f_{xy}^*(\omega)}{f_{yy}(\omega)}, \tag{5}$$

where

$$f_{xy}(\omega) = [f_{x_1y}(\omega) \ f_{x_2y}(\omega)] \tag{6}$$

$$f_{xx}(\omega) = \begin{bmatrix} f_{x_1x_1}(\omega) & f_{x_1x_2}^*(\omega) \\ f_{x_1x_2}(\omega) & f_{x_2x_2}(\omega) \end{bmatrix}$$

and $*$ now corresponds to the conjugate transpose. Equation 5 generalises for multivariate $\{x_t\}$. The equivalent metric in the time domain is the coefficient of determination for a multiple linear regression model.

Seasonally stratified power spectra are calculated as follows. Consider the time series x_s , defined as a 181-day subset of $\{x_t\}$ centred on $t = s$:

$$x_s = \{x_t | t = s - 90, \dots, s - 1, s, s + 1, \dots, s + 90\}. \quad (7)$$

All points in time occurring on February 29 are removed so that each year has exactly 365 days. The evolutionary power spectrum, as a function of both ω and s , is given by

$$f_{xy}(\omega, s) = \langle I_{xy}(\omega, s) \rangle \quad (8)$$

where the periodogram is given by $I_{xy}(\omega, s) = d_x(\omega, s) d_y^*(\omega, s)$ and $d_x(\omega, s)$ is the discrete Fourier transform of x_s . The seasonal power spectra $f_{xy}^S(\omega, n)$ is given by the averaging over all values of s which fall on the same day of each year n

$$f_{xy}^S(\omega, n) = \frac{\sum_{i=1}^N f_{xy}(\omega, 365(i-1) + n)}{N} \quad (9)$$

for $n = 1, 2, \dots, 365$

where N is the number of years in the series. In summary, power spectra are first calculated over 181-day subsets of $\{x_t\}$ with each successive block shifted by one day to yield the evolutionary spectrum. The seasonal power spectrum is then calculated by averaging across years for the same mid-date of the 181-day subsets (i.e., each January 1, January 2, etc).

References

- Antonov J, Seidov T, Boyer T, Locarnini R, Mishonov A, Garcia H, Baranova O, Zweng M, Johnson D (2010) World Ocean Atlas 2009, vol 2: salinity. U.S. Government Printing Office, Washington, DC
- Ascharyaphotha N, Wingwises P, Wongwises S, Humphries U, Xiaobao Y (2008) Simulation of seasonal circulation and thermohaline variabilities in the Gulf of Thailand. *Adv Atmos Sci* 25(3):489–506
- Blumberg A, Mellor G (1987) A description of a three-dimensional coastal ocean circulation model. *Three Dimens Coast Ocean Models* 4:1–16
- Csanady G (1982) *Circulation in the coastal ocean*. Springer, Berlin
- Doodson A (1928) The analysis of tidal observations. *Phil Trans R Soc Lond A* 227:223–279
- Fu L (2003) Wind-forced intraseasonal sea level variability of the extratropical oceans. *J Phys Oceanogr* 33(2):436–449
- Fu L (2007) Intraseasonal variability of the equatorial Indian Ocean observed from sea surface height, wind, and temperature data. *J Phys Oceanogr* 37(2):188–202
- Han W (2005) Origins and dynamics of the 90-day and 30–60-day variations in the equatorial Indian Ocean. *J Phys Oceanogr* 35(5):708–728
- Han W, Lawrence D, Webster P (2001) Dynamical response of equatorial Indian Ocean to intraseasonal winds: zonal flow. *Geophys Res Lett* 28(22):4215–4218
- Hormazabal S, Shaffer G, Pizarro O (2002) Tropical Pacific control of intraseasonal oscillations off Chile by way of oceanic and atmospheric pathways. *Geophys Res Lett* 29(6):1–4
- Hsu HH (2012) Intraseasonal variability in the atmosphere–ocean climate system. In: *Intraseasonal variability of the atmosphere–ocean–climate system: East Asian monsoon*, 2nd edn. Springer, Berlin, pp 73–104
- IOC, IHO, BODC (2003) Centenary edition of the GEBCO digital atlas, published on CDROM on behalf of the Intergovernmental Oceanographic Commission and the International Hydrographic Organization as part of the General Bathymetric Chart of the Oceans. British Oceanographic Data Centre, Liverpool
- Iskandar I, Mardiansyah W, Masumoto Y, Yamagata T (2005) Intraseasonal Kelvin waves along the southern coast of Sumatra and Java. *J Geophys Res* 110(C4):C04013
- Jin D, Waliser D, Jones C, Murtugudde R (2012) Modulation of tropical ocean surface chlorophyll by the Madden–Julian Oscillation. *Clim Dyn*. Accessed March 2012
- Kikuchi K, Wang B, Kajikawa Y (2012) Bimodal representation of the tropical intraseasonal oscillation. *Clim Dyn* 38:1989–2000
- Large W, Pond S (1981) Open ocean momentum flux measurements in moderate to strong winds. *J Phys Oceanogr* 11(3):324–336
- Lee JY, Wang B, Wheeler M, Fu X, Waliser D, Kang IS (2012) Real-time multivariate indices for the Boreal Summer Intraseasonal Oscillation over the Asian summer monsoon region. *Clim Dyn*. Accessed Oct 2012
- Locarnini R, Mishonov A, Antonov J, Boyer T, Garcia H, Baranova O, Zweng M, Johnson D (2010) World Ocean Atlas 2009, vol 1: temperature. U.S. Government Printing Office, Washington, DC
- Madden R, Julian P (1971) Detection of a 40–50 day oscillation in the zonal wind in the tropical Pacific. *J Atmos Sci* 28(5):702–708
- Madden R, Julian P (1972) Description of global-scale circulation cells in the tropics with a 40–50 day period. *J Atmos Sci* 29(6):1109–1123
- Maloney E, Kiehl J (2002) MJO-related SST variations over the tropical eastern Pacific during Northern Hemisphere summer. *J Clim* 15(6):675–689
- Maloney E, Chelton D, Esbensen S (2008) Subseasonal SST variability in the tropical eastern North Pacific during Boreal Summer. *J Clim* 21:4149–4167
- Matthews A, Singhruck P, Heywood K (2010) Ocean temperature and salinity components of the Madden–Julian oscillation observed by Argo floats. *Clim Dyn* 35(7–8):1149–1168
- Nagura M, McPhaden M (2012) The dynamics of wind-driven intraseasonal variability in the equatorial Indian Ocean. *J Geophys Res* 117(C2):C02001
- Oliver E (2011) Local and remote forcing of the ocean by the Madden–Julian Oscillation and its predictability. Ph.D. thesis, Dalhousie University, Halifax
- Oliver E, Thompson K (2010) Madden–Julian Oscillation and sea level: local and remote forcing. *J Geophys Res* 115(C1):C01003
- Oliver E, Thompson K (2011) Sea level and circulation variability of the Gulf of Carpentaria: influence of the Madden–Julian Oscillation and the adjacent deep ocean. *J Geophys Res* 116(C2):C02019
- Pawlowicz R, Beardsley B, Lentz S (2002) Classical tidal harmonic analysis including error estimates in MATLAB using T_TIDE. *Comput Geosci* 28(8):929–937
- Priestley M (1981) *Spectral analysis and time series*. Academic Press Inc., London
- Saha S, Moorthi S, Pan H, Wu X, Wang J, Nadiga S, Tripp P, Kistler R, Woollen J, Behringer D, et al (2010) The NCEP climate forecast system reanalysis. *Bull Am Meteorol Soc* 91(8):1015–1057
- Saha S, Moorthi M, Wu X, Wang J, Nadiga S, Tripp P (2012) The NCEP climate forecast system version 2. *J Clim* (submitted)
- Shaw PT, Chau SY (1994) Surface circulation in the South China Sea. *Deep Sea Res Part I* 41(11/12):1663–1683
- Shinoda T, Hendon H, Glick J (1998) Intraseasonal variability of surface fluxes and sea surface temperature in the tropical Western Pacific and Indian Oceans. *J Clim* 11(7):1685–1702

-
- Shumway R, Stoffer D (2000) Time series analysis and its applications. Springer, Berlin
- Webber B, Matthews A, Heywood K (2010) A dynamical ocean feedback mechanism for the Madden–Julian Oscillation. *Q J R Meteorol Soc* 136(648):740–754
- Wheeler M, Hendon H (2004) An all-season real-time multivariate MJO index: development of an index for monitoring and prediction. *Mon Weather Rev* 132(8):1917–1932
- Wheeler M, Hendon H, Cleland S, Meinke H, Donald A (2009) Impacts of the Madden–Julian oscillation on Australian rainfall and circulation. *J Clim* 22:1482–1498
- Zhang C (2005) Madden–Julian Oscillation. *Rev Geophys* 43:1–36
- Zhuang W, Xie SP, Wang D, Taguchi B, Aiki H, Sasaki H (2010) Intraseasonal variability in sea surface height over the South China Sea. *J Geophys Res* 115(C4):C04010